

A hybrid spectral-spatial fusion technique for hyperspectral object classification

Radhakrishna Mani, Manjunatha Raguttapalli Chowdareddy

Department of Electronics and Communication Engineering, Global Academy of Technology,
Affiliated to Visvesvaraya Technological University, Belagavi, India

Article Info

Article history:

Received Aug 8, 2023

Revised Sep 7, 2023

Accepted Nov 7, 2023

Keywords:

Deep learning

Fusion

Hyperspectral imaging

Machine learning

Multispectral

Object classification

ABSTRACT

In the field of object classification, hyperspectral imaging (HSI) has been widely used, due to its spectral-spatial, and temporal resolution of larger areas. The HSI is generally used to identify the objects physical properties in accurate manner and as well as to identify similar object with acceptable spectral signatures. Thus, the HSI has been widely used for object identification applications in different fields such as precision agriculture, environmental study, crop monitoring, and surveillance. However, the object classification is time consuming due to extremely large size; thus, the feature fusion of both spectral and spatial have been done. The current feature fusion method fails to retain semantic object intrinsic feature; further, current classification technique induces higher misclassification. In addressing the research issues this paper introduces a hybrid spectral-spatial fusion (HSSF) technique to reduce feature size and retains object intrinsic properties. Finally, in reducing misclassification a soft-margins kernel is introduced in support vector machine (SVM). Experiment is conducted on standard Indian Pines dataset; the result shows the HSSF-SVM model attain much higher accuracy and Kappa coefficient performance.

This is an open access article under the [CC BY-SA](https://creativecommons.org/licenses/by-sa/4.0/) license.



Corresponding Author:

Radhakrishna Mani

Research Scholar, Department of Electronics and Communication Engineering

Visvesvaraya technological university

Belagavi, Bengaluru, Karnataka, India

Email: rk123research@gmail.com

1. INTRODUCTION

Images captured through remote-sensing sensors, including those provided by satellites as well as unmanned-aerial-vehicles (UAVs), are known as remote-sensing images. Satellites are the primary source of global coverage, providing images of every single location on earth. Many fields, including forestry, agriculture, weather research, oceanography, as well as coastline research, make use of satellite imagery in this way. Particularly, it is put to good use in the fields of precision agricultural as well as in identification of phenotypes of plants [1], [2]. The normalized-difference vegetation-index (NDVI) [3] is one such indicator, and conventional approaches often employ the initial UAV multi-spectral (MS) image to derive the NDVI distributed mapping. Inaccuracy within the NDVI distributed mapping may result from the poor spatial resolution of the source MS images. In most cases, the spatial resolution of MS images is poor in comparison to the spectral resolution. Low spectral resolution and high spatial resolution are characteristics of hyperspectral images (HSI) and panchromatic (Pan) images as well as [4]. There is a clear loss of specific spatial information when using MS images. As a result, the spectral and spatial resolutions of the combined MS and HSI can be enhanced simultaneously. The resulting NDVI distributed mapping will have higher resolution and enhance

object classification performance; this development motivated the proposed research to develop an efficient hybrid fusion i.e., spatial-spectral fusion technique for performing object classification.

High resolution is one of the main conditions that must be met before the satellite images can be used for object classification applications. Images captured by hyperspectral sensors are rich in spectral-information but are poor in spatial-information. However, multispectral sensors are image sensors which capture both a large amount of geographical data and a small amount of spectral information. Image-fusion is a preprocessing method that improves both the spectral as well as the spatial resolution of an image. Image fusion method are utilized in a variety of fields as shown in Figure 1, including such as the visualization in the medical images, machine-vision [5], security in bioinformatics, classification of land, navigation, variation identification, digital imaging, military applications, satellite, and aerial imaging [6], [7], robotic vision, detection of food microbes [8], photography and surveillance [9]. The purpose of this research is to investigate recent developments in the field of image-fusion technique applied for object classification approaches using HSI and identify the problems and challenges encountered and present an effective feature fusion technique that retain object intrinsic characteristic both spatially and as well as spectrally.

In the image-fusion method [10], [11], considering two images from the same area captured by different sensors, the primary focus is on increasing the spectral and spatial resolution in one image without affecting object intrinsic characteristic information quality [12]. The current methods help produce a higher-resolution fusion image [13]; however, there is a possibility that the undesired artifacts as well as noise contents brought on by poor registration will have an effect on the overall appearance of the fused image in the original images [14]. Depending on the task at hand and the original image, the resulting fused image's improved quality will seem very different. The evaluation of the image quality is the single most important step in comprehending the relevance of the fusion process. Object classification applications have different needs, so it's crucial to select the right image fusion method [15]. Selecting the right approach for a remote sensing object classification implementation is difficult, particularly in the environment of supervised classification, where the "Hughes-phenomenon" is present due to an imbalance among the small size of training samples as well as the extremely high spectral dimensions of HSI, negatively impacting classification accuracy [10]–[15]. This paper introduces a hybrid fusion technique i.e., in this work feature fusion is done both spectrally and as well as spatially. Finally, the fused feature is used for performing object classification using machine learning algorithm namely support vector machine (SVM). The significance of the research work is given as:

- The work introduced a spectral feature fusion mechanism that reduces the overall bands required for performing object classification using hyperspectral imaging.
- Second, the work introduced spatial feature fusion mechanism that reduces and retain intrinsic features of each object.
- Finally, introduced a SVM classification algorithm that reduces misclassification using new soft-margin weights optimization.

In section 2, various existing image fusion and classification techniques are studied and identified its limitation for remote sensing object classification application. In section 3, presents proposed method of hybrid fusion technique. In section 4, provides experiment study and comparative analysis with existing fusion-based object classification methodology. Lastly, the research the concluded with future research direction.

2. LITERATURE SURVEY

This section studies recent fusion methodologies adopted for object classification. Pott *et al.* [16] designed HSI-based crop classification model using spatial information from HSI features. They used growing season data to model a transfer learning approach and examined precision in early-seasonal predictive approach; and lastly, crop classification is done to estimate large-scale crop area. Orynbaikyzy *et al.* [17] used multispectral time-series data combined with synthetic-aperture radar data for better crop-type mapping. They showed just using radar data exhibit poor accuracy, identified which feature combination increases accuracy, and studied misclassification for better crop profile modelling. They studied two fusion methodologies and showed feature selection aid in significantly reducing computational overhead.

Yin *et al.* [18] studied fusion methodology considering different view point for scene classification using HSI. They evaluated scene classification using single side image and also combination of multiple image [19]. Bouguettaya *et al.* [20] studied recent convolution neural network (CNN)-based crop classification approaches and its benefits for accurate results. Zhang [21] introduced a CNN combining interleaving perception for attaining better fusion; they model is focused in fusion of heterogenous information from light detection and ranging (LiDAR) data and HSI. In performing reconstruction of LiDAR and HSI features together designed a bidirectional autoencoder; finally, the two-branch CNN takes the fused information as input for performing classification.

Gao *et al.* [22] designed a land-cover recognition method of complex wetland which has mixed vegetation in patchy manner. First, the multispectral and HSI features are fused using CNN. The model assure good spatial-spectral feature resolution; then spatial and spectral visual correlation form fused image is used for performing pixel-wise object classification. Yang *et al.* [23] introduced fusion mechanism namely enhanced multiscale feature-fusion network (EMFFN). The model extract multiscale spatial-spectral features using two subnetworks namely spectral cascaded dilated convolutional network (SCDCN) and parallel multipath network (PMN) [24]. The SCDCN is used for extraction of multiscale features considering long-ranged information of larger fields. Then, PMN is used for capturing small, medium, and large-scale features spatially. Finally, feature are fused in hierarchical manner assuring better high-level semantic features considering limited training samples [25], [26].

3. PROPOSED METHOD

This section introduces a an effective HSI fusion technique that reduces the band and feature size and retains high quality feature both spatially and as well as spectrally. Finally, using the fused features information the object classification process is done using machine learning algorithm. The architecture of proposed HSI object classification methods is given in Figure 1.

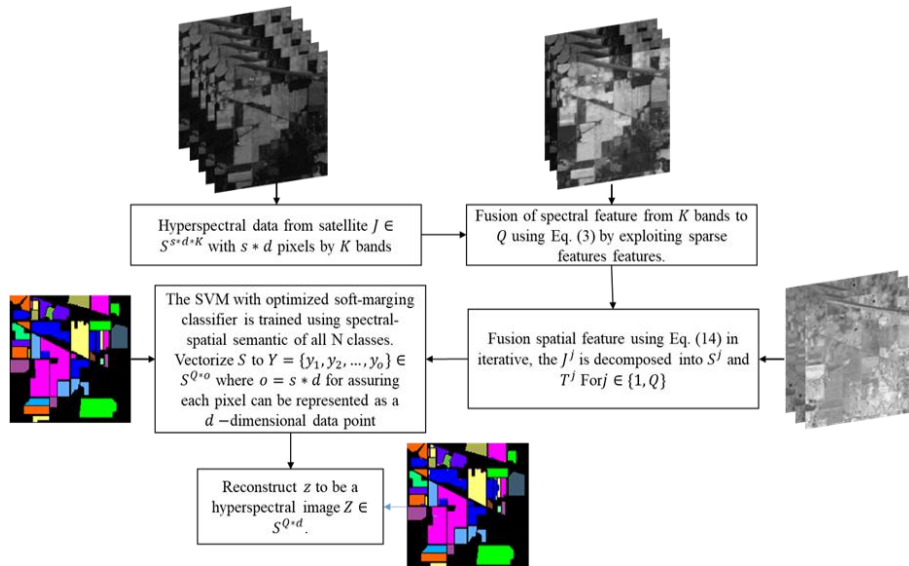


Figure 1. Architecture of prosed hybrid HSI fusion technique for object classification

3.1. Spectral feature fusion technique

The raw HSI J can be expressed using (1);

$$J = (J_1, \dots, J_O) \in \mathcal{S}^{C \times O} \tag{1}$$

where the raw HSI is segmented into N clusters with equal spectral band size, the parameter C defines dimensions and parameter O defines pixels size of raw HSI. The bands size in each cluster is expressed in (2);

$$C_1, C_2, \dots, C_N \tag{2}$$

the averaging-based image fusion is done at each group and the corresponding fusion data is given using (3);

$$\tilde{J}_n = \frac{\sum_{o=1}^{C_n} J_n^o}{C_n} \tag{3}$$

where parameter n defines the n th group, C_n defines the bands size in the n th group, J_n^o defines the o th band in the n th group of the raw HSI, and \tilde{J}_n defines the n th spectral band after performing fusion. In (3) enables the spectrally reduced pixels of HSI to retain the object physical properties i.e., quality of object reflectance

will be retained. Further, the model is very effective in eliminating noise. The spectrally reduced HSI \tilde{J} is again divided into multiple sub-clusters of neighboring bands as defined (4);

$$\hat{J}^l = \begin{cases} (\tilde{J}_{(l-1)A+1}, \dots, \tilde{J}_{(l-1)A+A}), & l = 1, 2, \dots, \lfloor \frac{N}{A} \rfloor \\ (\tilde{J}_{N-A+1}, \dots, \tilde{J}_N), & l = \lfloor \frac{N}{A} \rfloor + 1 \end{cases} \quad (4)$$

where \hat{J}^l defines to the l th subcluster, A defines bands size of each cluster, $\lfloor \frac{N}{A} \rfloor$ represent the minimum value not smaller than $\frac{N}{A}$, $\lceil \frac{N}{A} \rceil$ represent maximum value not larger than $\frac{N}{A}$. Then, for obtaining shading and reflectance features of each object optimization is done using intrinsic feature extraction mechanism at each subcluster \hat{J}^l as defined (5);

$$(T^{l*}, S^{l*}) = \arg \min_{S^l, T^l} E(\hat{J}^l, \hat{S}^l, \hat{T}^l) \quad (5)$$

where T^l defines shading elements of the l th subcluster and S^l defines reflectance elements of the l th subcluster. Finally, the reflectance features of objects in multiple subclusters are fused together for obtaining corresponding intrinsic features of objects, which is defined as a matrix representation with n -dimensional feature \tilde{S} as defined (6).

$$\tilde{S} = \begin{pmatrix} S^1 \\ \vdots \\ S^l \\ \vdots \\ S^{\lfloor \frac{N}{A} \rfloor} \end{pmatrix} \in \mathcal{S}^{N \times O} \quad (6)$$

3.2. Spatial feature fusion technique

In this section the work aimed at extracting features that retains objects intrinsic feature using minimum number of pixels. The intrinsic feature depends on the surface feature of earth; the illumination and climate condition impact the intrinsic properties of objects. In order to extract semantically meaningful features spatially the shading feature must be removed from the intrinsic feature. Let the intensity feature, intrinsic feature and shading feature be defined using parameter $J \in \mathcal{S}^{s \times d}$, $S \in \mathcal{S}^{s \times d}$, and $T \in \mathcal{S}^{s \times d}$, respectively. The HSI for a pixel q is expressed as a pixel-wise multiplicative of object reflectance and shading features as defined in (7);

$$J_q = S_q T_q, \quad (7)$$

where q represent pixel indexes. In (7), the parameter S_q and T_q are unknown parameter and J_q is the known parameter. The reflectance properties of objects will vary extremely at the edges and remain similar within the respective object class. The value of reflectance keeps changing with variation in intensity value; thus, identifying exact intensity value will result in identifying similar reflectance output. Therefore, reflectance S_q is measured in (8).

$$S_q = \sum_{r \in O(q)} b_{qr} S_r, \quad (8)$$

In (8) b_{qr} defines the parameter that estimates intensity similarities between spectral angle and intensity value among pixel indexes q and r as defined (9);

$$b_{qr} = e^{-(K_q - K_r)^2 / 2\sigma_{qK}^2 + A(J_q - J_r)^2 / \sigma_{qA}^2} \quad (9)$$

where parameter K is used to measure the intensity of HSI by taking the average of entire bands of HSI, σ_{qA} defines the difference in angle in local window in adjacent q and σ_{qK} defines the difference in intensities in local window in adjacent q . In (9) the angle between two-pixel vectors J_q and J_r represented by parameter $A(J_q - J_r)$ are measured using (10).

$$A(J_q - J_r) = \arccos (J_{qs}J_{rs} + J_{qg}J_{rg} + J_{qs}J_{rs}) \quad (10)$$

The parameter b_{qr} defines pairwise similarity between J_q and J_r and is an element of affinity matrix; where $\mathcal{O}(q)$ depicts the neighbor pixel q represented as Gaussian window as defined (11);

$$\mathcal{O}(q) = \exp\left(-\frac{\|q-r\|_2^2}{2\sigma^2}\right) \tag{11}$$

in (11) the size of σ and $\mathcal{O}(q)$ plays important role in obtaining semantic feature of objects intrinsic representation. In measuring b_{qr} affinity graph through gaussian function both range distance between intensity J_q and J_r and space distance between pixel q and r is used through (12);

$$b_{qr} = \begin{cases} \exp\left[-\left(\frac{\|q-r\|_2^2}{2\sigma_t^2} + \frac{\|J_q-J_r\|_2^2}{2\sigma_s^2}\right)\right], & \text{if } r \in \mathcal{O}(q) \\ 0, & \text{otherwise} \end{cases} \tag{12}$$

where σ_t defines the space optimization parameter and σ_s defines range optimization parameter. Therefore, using (12), the S_r can be established through (13).

$$S_r = \sum_{r \in \mathcal{O}(q)} \left\{ \exp\left[-\left(\frac{\|q-r\|_2^2}{2\sigma_t^2} + \frac{\|J_q-J_r\|_2^2}{2\sigma_s^2}\right)\right] \right\} S_r \tag{13}$$

Using (12) the HSI J_q structure can be preserved with better texture S_q representation. The object intrinsic feature is established by considering $\tilde{T}_q = \frac{1}{J_q}$ through linear properties using (7) and (8);

$$\begin{cases} S_q = \sum_{r \in \mathcal{O}(q)} b_{qr} S_r, \\ \tilde{T}_q = \frac{1}{J_q} S_r, \end{cases} \tag{14}$$

using (14), the value of S_r and T_q is approximated. Therefore, the reflectance value of different objects by eliminating shading is obtained. Thus, aiding in better spatial feature intrinsic representation. Once the fusion of both spectral and spatial is done. The final fused feature of S of different objects is represented as a vector form and trained using machine learning algorithm defined 3.3.

3.3. Object classification using machine learning algorithm

The classification problem of the object can be said to be a multi-objective classification. The supervised machine-learning algorithm, namely SVM has been used for the classification, regression and detection of the objects. Hence, in this work, we utilize the SVM for solving the multi-objective classification. In this proposed method, the SVM first builds hyper-planes or group of hyper-planes in a space which has the highest dimension. The structure of the hyper-planes can be acquired using [27]. The linear model for SVM hyper-plane is defined using the (15);

$$y = w^T \phi(X) + b \tag{15}$$

where, $\phi(X)$ is used for defining the space which has transformed features. Further, the margin is represented using the least distance between the decision hyper-plane and closest point using the dataset. To solve the multi-objective classification problem, it is important to build a hyper-plane which has a decision boundary which will help to increase the margin within the dataset. Hence, in the dataset, for every data-points, the target point represented as t_i should belong to $\{1, -1\}$, i.e., $t \in \{1, -1\}$. If the target point is satisfied, then it is said to linearly separable. When the target point does not satisfy, then it is said to be non-linearly separable. Hence, to address the issue of non-linearly separable, in this work, a soft-margin SVM has been presented which uses a slack parameter, $\varphi_i \geq 0$, where φ is used for defining the rate of misclassification. Moreover, when $\varphi_i > 1$, the data-points are said to be misclassified. Furthermore, the inequality constraints would arise which can be defined using the (16).

$$t_i(W_i^T \phi_i(X) + b) \geq 1 - \varphi_i \tag{16}$$

The inequality constraints arise because we try to change $y(x_n) > 0$ for the data-points having $t_n = 1$ and $y(x_n) < 0$ for the data-points having $t_n = -1$. The range between the data-point x_n and decision-boundary which is inside the hard-margin can be given using the (17);

$$\frac{t_n y(x_n)}{\|W\|} = \frac{t_i(W^T \phi(X) + b)}{\|W\|} \quad (17)$$

in finding the maximal margin or the best solution for the multi-objective classification, the (18) has to be solved;

$$\operatorname{argmax}_{W,b} \frac{1}{\|W\|} \min_n (t_n(W^T \phi(X) + b)) \quad (18)$$

by solving the (18) and the soft-margin slack parameter, the multi-objective problem changes to the given (19);

$$\operatorname{argmax}_{W,b,\varphi} \frac{1}{2} \|W\|^2 + C \sum_{n=1}^N \varphi_n \quad s.t. \quad t_n(W^T \phi(X) + b) \geq 1 - \varphi_n; \varphi_n \geq 0; n = 1, 2, \dots, N \quad (19)$$

where, the parameter C has been used as the regularization parameter which will help to control the trade-off among the margin as well as the misclassification-tolerance. Moreover, as the dataset which has been considered as non-linearly separable, the kernel method can be utilized for transforming it to a higher linear dimension, i.e., Gaussian Kernel method. Furthermore, the SVM handling a multi-objective classification is considered as a convex optimization issue, which can help the model to attain the best solution. By using the optimum decision boundary, the dataset can be classified into various labels. The results which have been discussed in the next section show that the proposed classification method for the hyperspectral image shows better performance in terms of accuracy and Kappa coefficient in comparison to other traditional classification methods.

4. RESULTS AND DISCUSSIONS

The performance of the HSSF-SVM based hyper-spectral image object classification using HSI has been compared with the other existing feature fusion-based object classification techniques spectral spatial dependent global learning (SSDGL) [10], central attention network (CAN) [11], convolution neural network - active learning-markov random field (CNN-AI-MNF) [12], enhanced-multiscale feature-fusion network (EMFFN) [23], 3-dimension self-attention multiscale feature-fusion network (3DSA-MFN) [24], adaptive spectral-spatial feature fusion network (ASSFFN) [25], low-rank attention multiple feature-fusion network (LMAFN) [26], and deep support vector machine (DSVM) [27]. For evaluating the proposed HSSF-SVM and other existing HSI object classification techniques, the Indian Pines dataset has been used. Overall-accuracy (OA), average-accuracy (AA), the kappa-coefficient (K), and time required for computation are some of the most commonly utilized metrics in current HSI-based object classification techniques to evaluate the effectiveness of various HSI fusion based object-classification approach. By attaining higher values for the OA, AA, and K, the technique shows the best performance. Moreover, by decreasing the time for the computation, the techniques can be deployed in the real-time.

4.1. Dataset description

An airborne visible/infrared imaging spectrometer (AVIRIS) sensor that was positioned over the northwestern corner of Indiana was used for capturing the data for the Indian-Pines dataset as shown in Figure 2. When gathering hyperspectral information, a wavelength of $0.4\text{-}2.5 \times 10^{-6}$ meters is used alongside 145×145 pixels and 224 bands. Indian-Pines dataset is necessary since two-thirds of the area that was measured is agricultural, while the remaining one-third is made up of forest along with other naturally present flora. In addition, there are crops that are still in the beginning phases of their development, which accounts for fewer than five percent of the total data acquired in Indian-Pines dataset. According to figure, there are an overall of 16 crops (or labels) that make up the ground-truth information. In a manner comparable to [2], [3], the water-absorption spectrum bands are removed, and the total number of the bands that comprise the spectral spectrum is decreased to 200.

4.2. Effect of hybrid fusion technique

In this section the impact that the hybrid-fusion technique has been given. The results for the accuracy attained for the classification when the HSSF is used by the proposed HSSF-SVM technique has been given in the Figure 3. The results for the accuracy attained for the classification when the SSF is not used by the proposed HSSF-SVM technique has been given in the Figure 3. When comparing it can be seen that the HSSF help to increase the accuracy for the classification of the HSIs. Hence, from all the results, it can be noted that the proposed HSSF-SVM technique has the ability to train the model and learn about the object features by removing the shadowing-element.

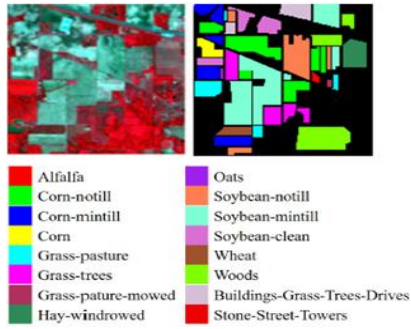


Figure 2. Pseudo-color image and ground-truth map for Indian Pines dataset

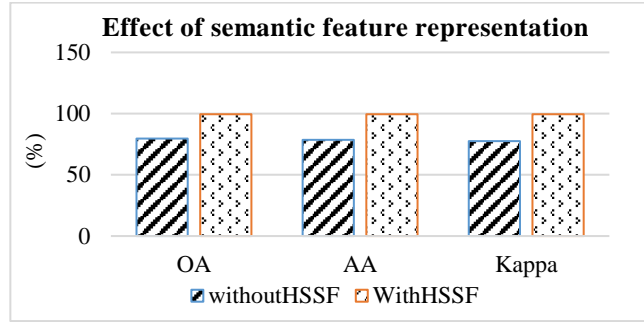


Figure 3. Effect of spatial-spectral fusion on hyperspectral object classification performance

4.3. Comparative study

In this section, the experimentation has been done using the Indian-Pines dataset and has been evaluated using the OA, AA, K and time required for the computation metrics. The proposed HSSF-SVM technique has been compared with the existing techniques like SSDGL, CAN, CNN-AI-MNF, EMFFN, 3DSA-MFN, LSGSAN, LMAFN, and DSVM techniques. The accuracy which has been achieved for the various objects (class name) has been given in Table 1. From the results presented in the Table 1, it can be noted that the presented HSSF-SVM technique attains the best accuracy in terms of OA, AA, K and time required for the computation for all the objects in comparison to the other existing techniques. Moreover, the proposed HSSF-SVM technique induces the least computing overhead when compared with all the CNN-AL-MNF and EMFFN technique.

Table 1. Comparative analysis

| Class name | DSVM (2020) [27] | CNN-AI-MNF (2020) [12] | SSDGL (2021) [10] | CAN (2021) [11] | EMFFN (2021) [23] | 3DSA-MFN (2022) [24] | ASSFFN (2022) [25] | LMAFN (2023) [26] | HHSSF-SVM [Proposed] |
|---------------------|------------------|------------------------|-------------------|-----------------|-------------------|----------------------|--------------------|-------------------|----------------------|
| Alfalfa | 100 | 92.71 | 100 | 87.8 | 100 | 98.67 | 93.18 | 98.78 | 100 |
| Corn notill | 100 | 92.98 | 99.63 | 98.05 | 96.88 | 99.59 | 96.24 | 64.40 | 99.98 |
| Corn mintill | 100 | 88.7 | 99.24 | 97.99 | 99.22 | 100.00 | 97.85 | 66.02 | 99.97 |
| Corn | 100 | 97.7 | 100 | 94.37 | 99.97 | 98.73 | 97.35 | 90.95 | 100 |
| Grass pasture | 99.43 | 92.9 | 99.56 | 98.39 | 99.37 | 100.00 | 98.91 | 83.37 | 99.56 |
| Grass trees | 98.89 | 98.89 | 100 | 99.7 | 99.80 | 99.54 | 99.71 | 96.72 | 99.88 |
| Grass pasture moved | 100 | 76.74 | 100 | 100 | 100 | 100.00 | 40.74 | 99.57 | 100 |
| Hay windrowed | 98.72 | 97.87 | 100 | 100 | 100 | 99.09 | 100 | 99.70 | 100 |
| Oats | 100 | 38.89 | 100 | 77.78 | 100 | 99.42 | 84.21 | 100.00 | 99.97 |
| Soybean notill | 95.75 | 92.27 | 99.68 | 98.17 | 98.07 | 99.56 | 96.86 | 74.01 | 99.41 |
| Soybean mintill | 100 | 95.07 | 99.36 | 98.33 | 97.91 | 100.00 | 98.67 | 67.36 | 99.46 |
| Soybean clean | 99.63 | 90.51 | 99.11 | 97.94 | 99.31 | 99.56 | 96.98 | 80.43 | 100 |
| wheat | 100 | 96.53 | 100 | 100 | 100 | 98.47 | 98.46 | 98.55 | 99.85 |
| woods | 100 | 99.28 | 100 | 98.77 | 99.53 | 98.73 | 100 | 93.01 | 100 |
| Buildings | 95.45 | 88.4 | 100 | 92.51 | 99.55 | 99.37 | 100 | 86.90 | 99.87 |
| Grass trees | | | | | | | | | |
| Stone steel | 100 | 97.12 | 100 | 98.81 | 99.73 | 99.37 | 98.88 | 98.30 | 100 |
| Towers | | | | | | | | | |
| OA (%) | 98.86 | 98.79 | 99.63 | 98.1 | 98.85 | 99.52 | 98.11 | 75.41 | 99.76 |
| AA (%) | 99.24 | 94.28 | 99.79 | 96.16 | - | 99.32 | 93.62 | 78.15 | 99.87 |
| Kappa (%) | - | - | 99.58 | 97.84 | 98.36 | 99.24 | 97.84 | 87.38 | 99.62 |
| Time (s) | - | 8109.34 | - | - | 279.65 | - | - | - | 67.5 |

4.4. Classification map comparizon

The Figure 4 shows the classification produced by existing HSI object classification methods. The accuracies of different existing HSI object classification methods is given inside the parenthesis. The result

clearly shows the proposed method produces very false positive in comparison with existing HSI object classification methods; thus, produces better classification maps in comparison with existing HSI object classification methods.

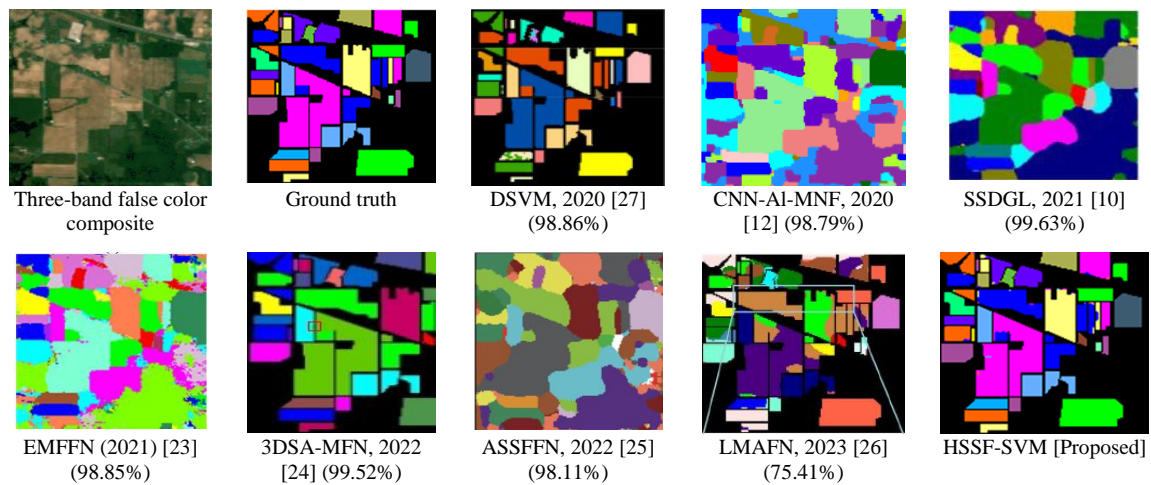


Figure 4. Classification maps produced using different HSI object classification methods

5. CONCLUSION

In this paper first various existing object classification model have been studied. The study shows the need for reducing the feature size to perform object classification; thus, various feature fusion mechanism has been presented to reduce the features both spatially and as well as spectrally. However, the study shows the current method failed to bring tradeoffs between reducing feature size and retaining object intrinsic characteristics. Further, the classification is a multi-label classification problem; the current method design classification with hard-margin. Thus, exhibit higher object misclassification. In this work a hybrid spectral-spatial fusion that reduce feature by eliminate shading element from object intrinsic features. Further, a soft-margin optimization for SVM is designed to attain better classification performance. Experiment is conducted using standard Indian Pines hyperspectral dataset; the result shows the HSSF-SVM attain much improved accuracy and kappa coefficient performance. The future work would further consider introducing realistic noise representing real-time environment and perform object classification and further, work on improving the model under noisy environment; alongside consider studying performance using different hyperspectral dataset.




REFERENCES

- [1] S. M. Panchal and S. Shivaputra, "Precise identification of objects in a hyperspectral image by characterizing the distribution of pure signatures," *International Journal of Electrical and Computer Engineering (IJECE)*, vol. 12, no. 6, p. 6068, Dec. 2022, doi: 10.11591/ijece.v12i6.pp6068-6078.
- [2] M. C. G. Baabu and P. M. C., "Semantic feature extraction method for hyperspectral crop classification," *Indonesian Journal of Electrical Engineering and Computer Science*, vol. 23, no. 1, p. 387, Jul. 2021, doi: 10.11591/ijeecs.v23.i1.pp387-395.
- [3] V. G. Vani and T. K., "Spatial-spectral feature for extraction technique for hyperspectral crop classification," *Indian Journal of Science and Technology*, vol. 15, no. 2, pp. 81–90, Jan. 2022, doi: 10.17485/IJST/v15i2.1810.
- [4] K. Zhang *et al.*, "Panchromatic and multispectral image fusion for remote sensing and earth observation: concepts, taxonomy, literature review, evaluation methodologies and challenges ahead," *Information Fusion*, vol. 93, pp. 227–242, May 2023, doi: 10.1016/j.inffus.2022.12.026.
- [5] M. C. G. Babu and P. M. C., "Inherent feature extraction and soft margin decision boundary optimization technique for hyperspectral crop classification," *International Journal of Advanced Computer Science and Applications*, vol. 12, no. 12, 2021, doi: 10.14569/IJACSA.2021.0121285.
- [6] A. Asokan, J. Anitha, B. Patrut, D. Danculescu, and D. J. Hemanth, "Deep feature extraction and feature fusion for bi-temporal satellite image classification," *Computers, Materials & Continua*, vol. 66, no. 1, pp. 373–388, 2020, doi: 10.32604/cmc.2020.012364.
- [7] O. Tamin, E. G. Mounq, J. A. Dargham, F. Yahya, and S. Omatu, "A review of hyperspectral imaging-based plastic waste detection state-of-the-arts," *International Journal of Electrical and Computer Engineering (IJECE)*, vol. 13, no. 3, p. 3407, Jun. 2023, doi: 10.11591/ijece.v13i3.pp3407-3419.
- [8] C.-H. Feng, Y. Makino, S. Oshita, and J. F. G. Martín, "Hyperspectral imaging and multispectral imaging as the novel techniques for detecting defects in raw and processed meat products: current state-of-the-art research advances," *Food Control*, vol. 84, pp. 165–176, Feb. 2018, doi: 10.1016/j.foodcont.2017.07.013.




- [9] S. Li, R. Dian, L. Fang, and J. M. Bioucas-Dias, "Fusing hyperspectral and multispectral images via coupled sparse tensor factorization," *IEEE Transactions on Image Processing*, vol. 27, no. 8, pp. 4118–4130, Aug. 2018, doi: 10.1109/TIP.2018.2836307.
- [10] Q. Zhu *et al.*, "A spectral-spatial-dependent global learning framework for insufficient and imbalanced hyperspectral image classification," *IEEE Transactions on Cybernetics*, vol. 52, no. 11, pp. 11709–11723, Nov. 2022, doi: 10.1109/TCYB.2021.3070577.
- [11] Z. Zhao, D. Hu, H. Wang, and X. Yu, "Center attention network for hyperspectral image classification," *IEEE Journal of Selected Topics in Applied Earth Observations and Remote Sensing*, vol. 14, pp. 3415–3425, 2021, doi: 10.1109/JSTARS.2021.3065706.
- [12] X. Cao, J. Yao, Z. Xu, and D. Meng, "Hyperspectral image classification with convolutional neural network and active learning," *IEEE Transactions on Geoscience and Remote Sensing*, vol. 58, no. 7, pp. 4604–4616, Jul. 2020, doi: 10.1109/TGRS.2020.2964627.
- [13] J. Li, K. Zheng, J. Yao, L. Gao, and D. Hong, "Deep unsupervised blind hyperspectral and multispectral data fusion," *IEEE Geoscience and Remote Sensing Letters*, vol. 19, pp. 1–5, 2022, doi: 10.1109/LGRS.2022.3151779.
- [14] H. Guo, W. Bao, K. Qu, X. Ma, and M. Cao, "Multispectral and hyperspectral image fusion based on regularized coupled non-negative block-term tensor decomposition," *Remote Sensing*, vol. 14, no. 21, p. 5306, Oct. 2022, doi: 10.3390/rs14215306.
- [15] L. Zhang, X. Zhang, M. Peng, X. Sun, and X. Zhao, "Hyperspectral data fusion using multidimensional information," in *Advances in Hyperspectral Image Processing Techniques*, Wiley, 2022, pp. 293–340. doi: 10.1002/9781119687788.ch11.
- [16] L. P. Pott, T. J. C. Amado, R. A. Schwalbert, G. M. Corassa, and I. A. Ciampitti, "Satellite-based data fusion crop type classification and mapping in rio grande do sul, Brazil," *ISPRS Journal of Photogrammetry and Remote Sensing*, vol. 176, pp. 196–210, Jun. 2021, doi: 10.1016/j.isprsjprs.2021.04.015.
- [17] A. Orynbaikyzy, U. Gessner, B. Mack, and C. Conrad, "Crop type classification using fusion of sentinel-1 and sentinel-2 data: assessing the impact of feature selection, optical data availability, and parcel sizes on the accuracies," *Remote Sensing*, vol. 12, no. 17, p. 2779, Aug. 2020, doi: 10.3390/rs12172779.
- [18] L. Yin, P. Yang, K. Mao, and Q. Liu, "Remote sensing image scene classification based on fusion method," *Journal of Sensors*, vol. 2021, pp. 1–14, Jun. 2021, doi: 10.1155/2021/6659831.
- [19] Z. Huang and S. Xie, "Classification method for crop by fusion hyper spectral and LiDAR data," in *2022 14th International Conference on Measuring Technology and Mechatronics Automation (ICMTMA)*, IEEE, Jan. 2022, pp. 1011–1014. doi: 10.1109/ICMTMA54903.2022.00205.
- [20] A. Bouguettaya, H. Zarzour, A. Kechida, and A. M. Taberkit, "Deep learning techniques to classify agricultural crops through UAV imagery: a review," *Neural Computing and Applications*, vol. 34, no. 12, pp. 9511–9536, Jun. 2022, doi: 10.1007/s00521-022-07104-9.
- [21] M. Zhang, W. Li, R. Tao, H. Li, and Q. Du, "Information fusion for classification of hyperspectral and LiDAR data using IP-CNN," *IEEE Transactions on Geoscience and Remote Sensing*, vol. 60, pp. 1–12, 2022, doi: 10.1109/TGRS.2021.3093334.
- [22] Y. Gao *et al.*, "Fusion classification of HSI and MSI using a spatial-spectral vision transformer for wetland biodiversity estimation," *Remote Sensing*, vol. 14, no. 4, p. 850, Feb. 2022, doi: 10.3390/rs14040850.
- [23] J. Yang, C. Wu, B. Du, and L. Zhang, "Enhanced multiscale feature fusion network for HSI classification," *IEEE Transactions on Geoscience and Remote Sensing*, vol. 59, no. 12, pp. 10328–10347, Dec. 2021, doi: 10.1109/TGRS.2020.3046757.
- [24] Y. Qing, Q. Huang, L. Feng, Y. Qi, and W. Liu, "Multiscale feature fusion network incorporating 3D self-attention for hyperspectral image classification," *Remote Sensing*, vol. 14, no. 3, p. 742, Feb. 2022, doi: 10.3390/rs14030742.
- [25] H. Gao, Z. Chen, and F. Xu, "Adaptive spectral-spatial feature fusion network for hyperspectral image classification using limited training samples," *International Journal of Applied Earth Observation and Geoinformation*, vol. 107, p. 102687, Mar. 2022, doi: 10.1016/j.jag.2022.102687.
- [26] F. Feng, Y. Zhang, J. Zhang, and B. Liu, "Low-rank constrained attention-enhanced multiple spatial-spectral feature fusion for small sample hyperspectral image classification," *Remote Sensing*, vol. 15, no. 2, p. 304, Jan. 2023, doi: 10.3390/rs15020304.
- [27] O. Okwuashi and C. E. Ndehedehe, "Deep support vector machine for hyperspectral image classification," *Pattern Recognition*, vol. 103, p. 107298, Jul. 2020, doi: 10.1016/j.patcog.2020.107298.

BIOGRAPHIES OF AUTHORS



Radhakrishna Mani    he is a research scholar, Department of Electronics and Communication Engineering, Visvesvaraya Technological University, Karnataka, India. He completed B.E. in VTU, Karnataka and M. Tech. from JNTU, Hyderabad. Area of interest artificial intelligence, deep learning, machine learning, data mining, and image processing. He can be contacted at email: rk123research@gmail.com.



Manjunatha Raguttapalli Chowdareddy    he is an associate Professor at Global Academy of Technology in Electronics and Communication Engineering Department. He holds a Ph.D. from Jain University, with his extensive knowledge and experience, he actively contributes to the Department of Electronics and Communication Engineering, enriching the learning experience for students and making significant contributions to the field of electronics and communication engineering. He can be contacted at email: manjunathrc84@gmail.com.